

Article

# Investigation of Various Pd Species in Pd/BEA for Cold Start Application

Beibei Zhang <sup>1</sup>, Meiqing Shen <sup>1,2,3</sup>, Jianqiang Wang <sup>1</sup>, Jiaming Wang <sup>4</sup> and Jun Wang <sup>1,\*</sup>

<sup>1</sup> Key Laboratory for Green Chemical Technology of State Education Ministry, School of Chemical Engineering & Technology, Tianjin University, Tianjin 300072, China; zhang\_525@tju.edu.cn (B.Z.); mqshen@tju.edu.cn (M.S.); jianqiangwang@tju.edu.cn (J.W.)

<sup>2</sup> State Key Laboratory of Engines, Tianjin University, Tianjin 300072, China

<sup>3</sup> Collaborative Innovation Center of Chemical Science and Engineering, Tianjin 300072, China

<sup>4</sup> Wuxi Weifu Lida Catalytic Converter Co., Ltd., Wuxi 214028, China; jiaming.wang@weifu.com.cn

\* Correspondence: wangjun@tju.edu.cn; Tel.: +86-22-2740-7002

Received: 16 February 2019; Accepted: 4 March 2019; Published: 7 March 2019



**Abstract:** A series of Pd/BEA catalysts with various Pd loadings were synthesized. Two active Pd<sup>2+</sup> species, Z<sup>-</sup>-Pd<sup>2+</sup>-Z<sup>-</sup> and Z<sup>-</sup>-Pd(OH)<sup>+</sup>, on exchanged sites of zeolites, were identified by in situ FTIR using CO and NH<sub>3</sub> respectively. Higher NO<sub>x</sub> storage capacity of Z<sup>-</sup>-Pd<sup>2+</sup>-Z<sup>-</sup> was demonstrated compared with that of Z<sup>-</sup>-Pd(OH)<sup>+</sup>, which was caused by the different resistance to H<sub>2</sub>O. Besides, lower Pd loading led to a sharp decline of Z<sup>-</sup>-Pd(OH)<sup>+</sup>, which was attributed to the ‘exchange preference’ for Z<sup>-</sup>-Pd<sup>2+</sup>-Z<sup>-</sup> in BEA. Based on this research, the atom utilization of Pd can be improved by decreasing Pd loading.

**Keywords:** Pd/BEA; Cold start; Pd species; NO<sub>x</sub> abatement

## 1. Introduction

The exhaust regulation on NO<sub>x</sub> emissions is getting more stringent [1]. Presently, NH<sub>3</sub> selective catalytic reduction (SCR) [2] and NO<sub>x</sub> storage reduction (NSR) [3] are widely used for NO<sub>x</sub> removal. However, standard NO<sub>x</sub> aftertreatment technologies fail to function efficiently at low temperatures, which results in a large proportion of the tailpipe NO<sub>x</sub> emission [4]. Meanwhile, high efficiency internal combustion engines require new and/or improved technologies which specifically address their low exhaust temperatures. In response to difficulties of low temperature emissions control, numerous efforts are underway to develop catalysts that light-off at temperatures below 150 °C. Passive NO<sub>x</sub> adsorbers (PNAs) could play a critical role in enabling high efficiency advanced combustion systems.

Recently, Pd/zeolite serving as passive NO<sub>x</sub> adsorbers (PNAs) was first proposed by Chen et al. [4]. This catalyst is emerging as effective passive NO<sub>x</sub> adsorbent technology because of its NO<sub>x</sub> storage/release capabilities, resistance to sulfur poisoning and hydrothermal deactivation [4–8]. Due to these excellent characteristics, Pd/zeolite has attracted great interest recently and has been further optimized [6–18].

Several recent studies show that isolated Pd ions in Pd/zeolite are the main active sites for NO<sub>x</sub> trapping [6,7,11,13,16]. It is reported that there are nine skeletal T sites with various chemical environments in BEA [19]. So, isolated Pd ions located in various positions of zeolite framework are likely to be formed. As reported by Gao et al. and Giordanino et al. [20–22], two kinds of isolated Cu species (Cu<sup>2+</sup> and [Cu(OH)]<sup>+</sup>) are identified on various framework positions of Cu/SSZ-13, which indicates that species of isolated cations may be influenced by their locations in zeolites. They also mentioned that Cu species were significantly affected by Cu loading. So, various isolated Pd species may co-exist in Pd/BEA, and Pd loading may be capable of influencing the content of them. Actually,

two kinds of active isolated Pd ions (bare Pd<sup>2+</sup> and Pd(OH)<sup>+</sup>) have been observed by Zheng et al. [10] and Khivantsev et al. [12]. However, they did not point out the difference in adsorption between these two species.

Therefore, these two kinds of isolated Pd ions were further studied in this research. A series of in situ FTIR experiments in CO and NH<sub>3</sub> were carried out, and a semiquantitative method was adopted to distinguish these two species. Based on this method, the NO<sub>x</sub> storage capacity of each isolated Pd species was compared. Further, by increasing the proportion of isolated Pd species with higher NO<sub>x</sub> storage capacities, the atom utilization of Pd can be improved.

## 2. Results

### 2.1. Ex-Situ FTIR

Ex-situ FTIR spectra of each sample are exhibited in Figure 1. Compared with 0-Pd (Figure 1a), an extra vibration at 926 cm<sup>-1</sup> is observed on the FTIR spectrum of 1-Pd. This peak is attributed to the vibration distortion of the skeletal T–O–T bond due to the strong interaction of Pd ions [4]. This is an obvious piece of evidence for the existence of Pd ions on the exchange sites of zeolites. Peaks at 926 cm<sup>-1</sup> appear on spectra of 0.2-Pd, 0.5-Pd and 2-Pd, too (Figure 1b). So, the existence of Pd ions on exchange sites in these samples is confirmed.

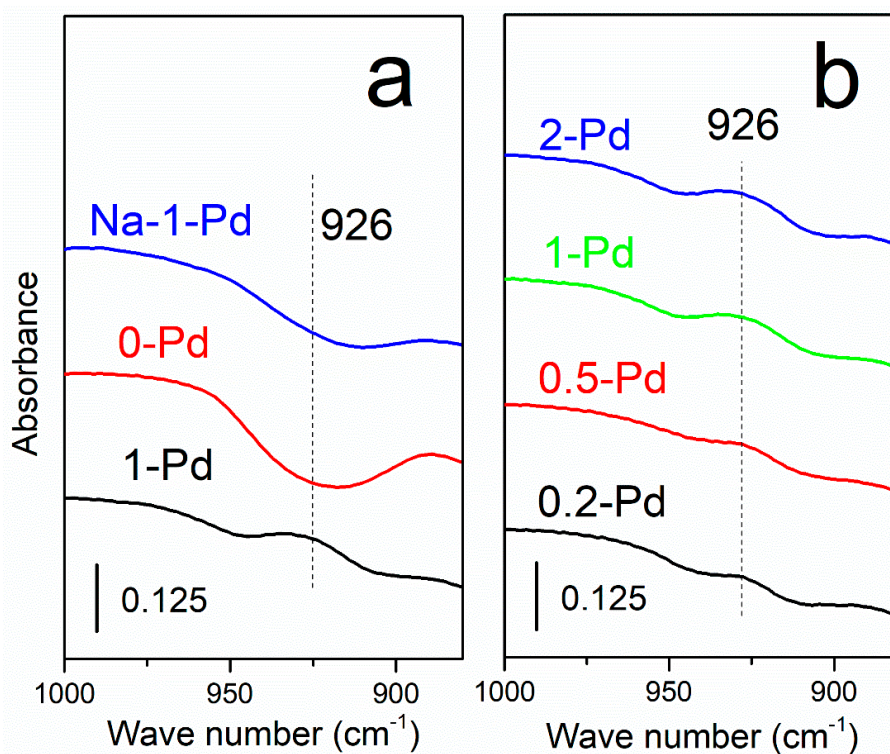


**Figure 1.** (a) Ex-situ FTIR spectra of 0-Pd, 1-Pd, Na-1-Pd; (b) Ex-situ FTIR spectra of 2-Pd, 1-Pd, 0.5-Pd, 0.2-Pd (Temperature: 200 °C; Flow: N<sub>2</sub>, 1 L/min).

Compared with 1-Pd (Figure 1a), the peak at 926 cm<sup>-1</sup> disappears in the spectrum of Na-1-Pd, which indicates the elimination of isolated Pd ions on exchange sites. This is firm evidence of which isolated Pd ions in Na-1-Pd have been completely exchanged by Na<sup>+</sup> ions through the titration process. So, Pd loaded on Na-1-Pd mainly exists in form of Pd oxidations.

## 2.2. Na<sup>+</sup> Titration

Na<sup>+</sup> titration was adopted to measure the content of isolated Pd ions in each sample [23], and the proportion of isolated Pd ions in total Pd loading (marked as Isolated Pd/Pd loading in Table 1) was further calculated. Considering that Pd is sensitive to Cl [24,25], the titration process was carried out in a NaNO<sub>3</sub> solution. Besides, this measurement is believed to have no negative effect on zeolite structures since the titration process was carried out in mild conditions and no calcination was done. As shown in Table 1, lower Pd loading leads to less isolated Pd<sup>2+</sup> content, whereas the proportion of isolated Pd ions in total Pd loading becomes larger. This phenomenon indicates that the increase of Pd loading leads to the formation of more Pd oxidations (PdOx), which is consistent with Jaeha Lee et al.'s study [11].

**Table 1.** The content of Pd ions on exchange sites of each sample.

Catalyst	0-Pd	0.2-Pd	0.5-Pd	1-Pd	2-Pd
Isolated Pd (wt %)	0.00	0.22	0.53	0.87	0.91
Isolated Pd/Pd loading (%)	0.00	95.7	96.4	77.7	42.7

## 2.3. CO In Situ FTIR

Pd species were further probed by CO using in situ FTIR, and the result is displayed in Figure 2. Peaks below 2100 cm<sup>-1</sup> are attributed to CO signals on metallic Pd (Pd<sup>0</sup>) formed via CO reduction [10,26], among which Pd<sup>0</sup>-CO (atop) are found at 2098 cm<sup>-1</sup>, 2076 cm<sup>-1</sup> and Pd<sub>2</sub><sup>0</sup>-CO (bridging) are found at 1951 cm<sup>-1</sup>. Besides, the peak at 2117 cm<sup>-1</sup> is attributed to the C-O vibration on Pd<sup>+</sup> [10,27]. As reported by Vu et al. [9], Pd<sup>+</sup> is formed by the CO reduction of ion-exchanged Pd species [9]. CO signals on isolated Pd<sup>2+</sup> species are observed above 2100 cm<sup>-1</sup>. The peak at 2152 cm<sup>-1</sup> with a shoulder peak at 2137 cm<sup>-1</sup> is attributed to the C-O vibration on isolated Pd<sup>2+</sup> bonded with the hydroxy of zeolites (marked as Z<sup>-</sup>-Pd<sup>2+</sup>-Z<sup>-</sup>) [10]. The peak at 2179 cm<sup>-1</sup> is attributed to the vibration of C-O adsorbed by another kind of isolated Pd<sup>2+</sup> [10], which was first determined as Z<sup>-</sup>-Pd(OH)<sup>+</sup> by Okumura et al. [28].

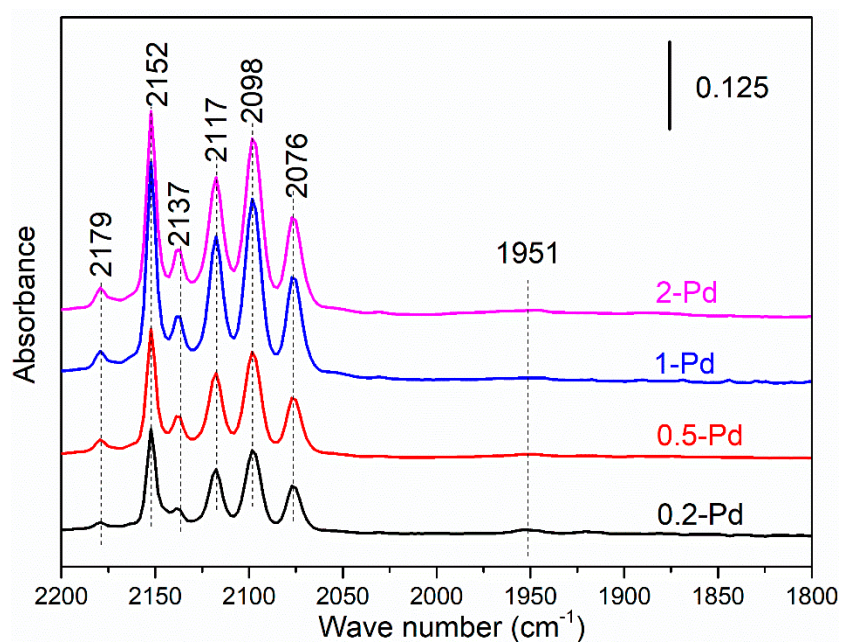


**Figure 2.** CO in situ FTIR spectra of 2-Pd, 1-Pd, 0.5-Pd, 0.2-Pd (Temperature: 80 °C; Flow: 1000 ppm CO, balanced with N<sub>2</sub>, 500 mL/min).

In short, two kinds of isolated  $\text{Pd}^{2+}$  ( $\text{Z}^- - \text{Pd}^{2+} - \text{Z}^-$  and  $\text{Z}^- - \text{Pd}(\text{OH})^+$ ) were identified in 0.2-Pd, 0.5-Pd, 1-Pd and 2-Pd. Note that all spectra in Figure 2 were obtained when the steady state had been achieved, and corresponding peaks of  $\text{Z}^- - \text{Pd}^{2+} - \text{Z}^-$  and  $\text{Z}^- - \text{Pd}(\text{OH})^+$  were still observed. So, these two isolated  $\text{Pd}^{2+}$  species cannot be completely reduced by CO at this temperature, which indicated that the reduction reaction is a reversible one. As shown in Figure S1, the existence of  $\text{Z}^- - \text{Pd}^{2+} - \text{Z}^-$  in 1-Pd-80 is also demonstrated by CO whereas no  $\text{Z}^- - \text{Pd}(\text{OH})^+$  is observed. Since the complete reduction of  $\text{Z}^- - \text{Pd}(\text{OH})^+$  cannot be achieved by CO, there is only one isolated  $\text{Pd}^{2+}$  species,  $\text{Z}^- - \text{Pd}^{2+} - \text{Z}^-$ , in 1-Pd-80 (see Figure S1).

#### 2.4. Catalyst Evaluation

Profiles of the  $\text{NO}_x$  adsorption stage are shown in Figure 3.  $\text{NO}_x$  storage capacities are calculated by the integration of negative peaks on these profiles, and the dead volume has been subtracted. The result is displayed in Table 2. Note that samples with the same Pd loading as much as 1 wt % (see Figure S2) exhibit entirely different  $\text{NO}_x$  storage capacities ( $53.3 \mu\text{mol/gcat}$  and  $9.9 \mu\text{mol/gcat}$  respectively), which indicates that only part of Pd loaded on samples is efficient. As shown in Figure 3,  $\text{NO}_x$  storage capacities of 0-Pd and Na-1-Pd are very low. So, Brønsted hydroxyl group and  $\text{PdO}_x$  are inefficient active centers for  $\text{NO}_x$  storage, whereas they do trap  $\text{NO}_x$  in this condition as reported [10,27]. Since the  $\text{NO}_x$  storage capacity of 1-Pd is much higher, isolated  $\text{Pd}^{2+}$  ions are likely to be the main active sites for  $\text{NO}$  trapping.

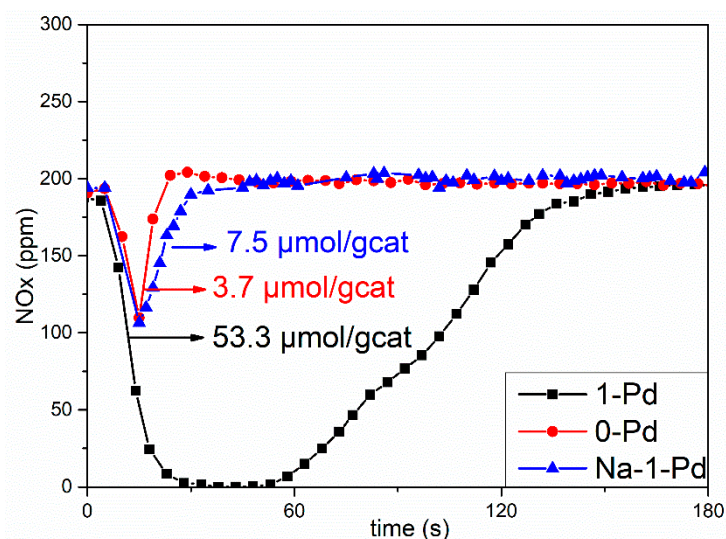


**Figure 3.**  $\text{NO}_x$  adsorption profiles (Temperature:  $80^\circ\text{C}$ ; Flow:  $\text{NO}_x$ ,  $\text{CO}$ ,  $\text{H}_2\text{O}$ ,  $\text{O}_2$ ,  $\text{CO}_2$ , balanced with  $\text{N}_2$ , 1 L/min).

**Table 2.**  $\text{NO}_x$  storage capacities in  $\text{NO}_x$ ,  $\text{CO}$ ,  $\text{H}_2\text{O}$ ,  $\text{O}_2$  and  $\text{CO}_2$ .

Catalyst	0-Pd	0.2-Pd	0.5-Pd	1-Pd	2-Pd
$\text{NO}_x$ storage capacity ( $\mu\text{mol/gcat}$ )	3.7	21.6	47.5	53.3	50.1

#### 2.5. $\text{NH}_3$ In Situ FTIR

Acidity over samples is probed by  $\text{NH}_3$  with in situ FTIR, and the result is exhibited in Figure 4. The peak at  $1463\text{cm}^{-1}$  observed in both spectra of 1-Pd and 0-Pd (Figure 4a) is attributed to the vibration of  $\text{NH}_4^+$  in Brønsted hydroxyl groups ( $\text{NH}_4^+ - \text{B}$ ) [29]. In the spectrum of 1-Pd, two additional peaks at  $1625\text{cm}^{-1}$  and  $1313\text{cm}^{-1}$  corresponding to the vibration of  $\text{NH}_3$  on Lewis acid ( $\text{NH}_3 - \text{L}$ ) [30,31] is observed. Nevertheless, these two peaks do not exist in Na-1-Pd in which isolated  $\text{Pd}^{2+}$  ions

( $Z^- - Pd^{2+} - Z^-$  and  $Z^- - Pd(OH)^+$ ) are replaced by  $Na^+$  completely. So, it is reasonable to believe that Lewis acid is generated from  $Z^- - Pd^{2+} - Z^-$  and  $Z^- - Pd(OH)^+$  species.

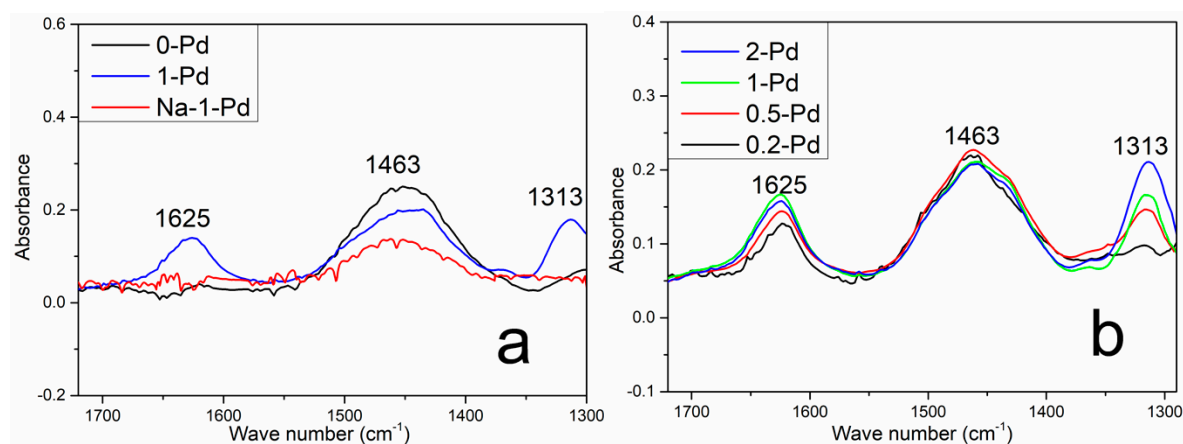


**Figure 4.** (a)  $NH_3$  in situ FTIR spectra of 0-Pd, 1-Pd, Na-1-Pd; (b)  $NH_3$  in situ FTIR spectra of 2-Pd, 1-Pd, 0.5-Pd, 0.2-Pd (Temperature: 80 °C; Flow: 500 ppm  $NH_3$ , balanced with  $N_2$ , 500 mL/min).

As shown in Figure S3, there is only one peak at  $1625\text{cm}^{-1}$  corresponding to the vibration of  $NH_3-L$  observed in the spectrum of 1-Pd-80. Since there is only one kind of isolated  $Pd^{2+}$ ,  $Z^- - Pd^{2+} - Z^-$ , in this sample as discussed above, the peak at  $1625\text{cm}^{-1}$  should be assigned to the vibration of  $NH_3-L$  originated from  $Z^- - Pd^{2+} - Z^-$ . In this case, the peak at  $1313\text{cm}^{-1}$  should be attributed to the vibration of  $NH_3-L$  originating from  $Z^- - Pd(OH)^+$ .

Since  $Z^- - Pd^{2+} - Z^-$  and  $Z^- - Pd(OH)^+$  are capable of being probed by  $NH_3$ , the ratio of the height of the peaks at  $1625\text{cm}^{-1}$  ( $P_{Z^- - Pd^{2+} - Z^-}$ ) and  $1313\text{cm}^{-1}$  ( $P_{Z^- - Pd(OH)^+}$ ) in Figure 4b can be defined as the relative content between these two isolated  $Pd^{2+}$  species. Considering that extinction coefficients for  $NH_3$  molecules adsorbed on  $Z^- - Pd^{2+} - Z^-$  and  $Z^- - Pd(OH)^+$  are both constants, they have no effect on the tendency of peak height ratios. So, the extinction coefficient is not considered in this part [32–34]. The result is shown in Figure 5a. It is worth nothing that  $P_{Z^- - Pd(OH)^+} / P_{Z^- - Pd^{2+} - Z^-}$  rises in parallel with the increase of isolated  $Pd^{2+}$ , which means that the higher content of isolated  $Pd^{2+}$  leads to a much more obvious increase of  $Z^- - Pd(OH)^+$  than that of  $Z^- - Pd^{2+} - Z^-$ . So, isolated  $Pd^{2+}$  in 0.2-Pd mainly exists in the form of  $Z^- - Pd^{2+} - Z^-$ , whereas a large amount of  $Z^- - Pd(OH)^+$  ions are formed in 2-Pd.

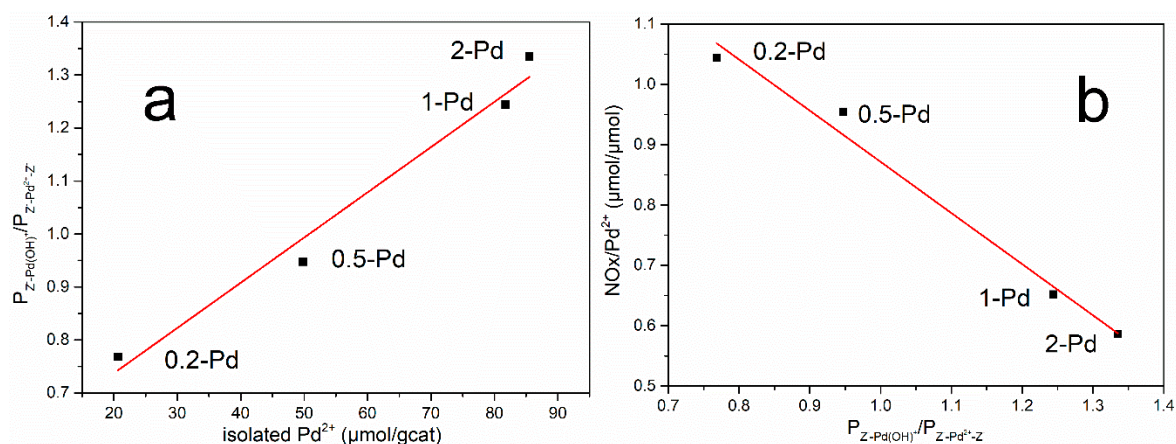


**Figure 5.** (a) tendency between isolated  $Pd^{2+}$  and  $P_{Z^- - Pd(OH)^+} / P_{Z^- - Pd^{2+} - Z^-}$ ; (b) tendency between  $P_{Z^- - Pd(OH)^+} / P_{Z^- - Pd^{2+} - Z^-}$  and  $NO_x / Pd^{2+}$ .

Mole ratios of  $\text{NO}_x$  adsorbed to isolated  $\text{Pd}^{2+}$  for each sample (marked as  $\text{NO}/\text{Pd}^{2+}$ ) are calculated via data in Tables 1 and 2. Figure 5b is plotted by  $\text{P}_{\text{Z}^- - \text{Pd}(\text{OH})^+} / \text{P}_{\text{Z}^- - \text{Pd}^{2+} - \text{Z}^-}$  on the horizontal axis and  $\text{NO}_x/\text{Pd}^{2+}$  on the vertical. As reported,  $\text{NO}_x$  is believed to be trapped in the form of  $\text{Pd}^{\text{II}}-\text{NO}$  [12,15], so the maximum  $\text{NO}_x/\text{Pd}^{2+}$  ratio is 1 in theory. However, the downward trend between  $\text{P}_{\text{Z}^- - \text{Pd}(\text{OH})^+} / \text{P}_{\text{Z}^- - \text{Pd}^{2+} - \text{Z}^-}$  and  $\text{NO}_x/\text{Pd}^{2+}$  means that higher  $\text{P}_{\text{Z}^- - \text{Pd}(\text{OH})^+} / \text{P}_{\text{Z}^- - \text{Pd}^{2+} - \text{Z}^-}$  leads to lower  $\text{NO}_x$  storage capacity of isolated  $\text{Pd}^{2+}$ , which indicates that the  $\text{NO}_x$  storage capacity of  $\text{Z}^- - \text{Pd}(\text{OH})^+$  is obviously lower than that of  $\text{Z}^- - \text{Pd}^{2+} - \text{Z}^-$  in this condition.

A further discussion is given below so as to give a reasonable explanation from the perspective of the structure-function relationship.

In BEA zeolite, nine skeletal T sites with various chemical environments are determined [19]. Among these T sites, T5 and T6 are demonstrated to have the lowest Al substitution energy [35]. Thus, Al substitution on these two sites (marked as  $\text{Al}_{\text{T5}}$  and  $\text{Al}_{\text{T6}}$ ) is preferential, and the amount of  $\text{Al}_{\text{T5}}$  and  $\text{Al}_{\text{T6}}$  is larger than that of Al atoms on the other T sites in BEA. Besides, exchange sites formed on these two Al atoms are more active due to the lowest deprotonation energy [36] of them. Meanwhile,  $\text{Al}_{\text{T5}}$  and  $\text{Al}_{\text{T6}}$  are located in the meta-position of the same five-membered ring [37], and the co-ion-exchange of protons on these two exchange sites formed on  $\text{Al}_{\text{T5}}$  and  $\text{Al}_{\text{T6}}$  is feasible. These characteristics of BEA can explain the 'exchange preference' for  $\text{Z}^- - \text{Pd}^{2+} - \text{Z}^-$  formed in Pd/BEA with lower content of isolated Pd ions to some extent. Besides, with the increase of Pd loading, more exchange sites are taken up. Limited by the amount of protons which are capable of being exchanged,  $\text{Z}^- - \text{Pd}(\text{OH})^+$  ions, which take up less exchange sites than  $\text{Z}^- - \text{Pd}^{2+} - \text{Z}^-$ , are preferred to be formed. So, higher content of isolated  $\text{Pd}^{2+}$  leads to much more obvious increase of  $\text{Z}^- - \text{Pd}(\text{OH})^+$  than that of  $\text{Z}^- - \text{Pd}^{2+} - \text{Z}^-$ .

As discussed above, the maximum  $\text{NO}_x/\text{Pd}^{2+}$  ratio is 1 in theory. As reported by Khivantsev et al. [12],  $\text{H}_2\text{O}$  molecules can occupy  $\text{NO}_x$  storage sites due to strong hydration of isolated  $\text{Pd}^{2+}$  species. Since isolated  $\text{Pd}^{2+}$  is the main active site for  $\text{NO}_x$  storage, the  $\text{NO}_x/\text{Pd}^{2+}$  ratio of Pd/zeolite-based PNA materials will significantly smaller than 1 in the presence of  $\text{H}_2\text{O}$ . However, as shown in Figure 5b,  $\text{NO}_x/\text{Pd}^{2+}$  of 0.2-Pd is as much as 1, which indicates that isolated  $\text{Pd}^{2+}$  in this sample is not occupied by  $\text{H}_2\text{O}$ . As discussed above, isolated  $\text{Pd}^{2+}$  in 0.2-Pd mainly exists in the form of  $\text{Z}^- - \text{Pd}^{2+} - \text{Z}^-$ . Thus  $\text{Z}^- - \text{Pd}^{2+} - \text{Z}^-$  may be insensitive to  $\text{H}_2\text{O}$  in this condition. Furthermore,  $\text{Z}^- - \text{Pd}(\text{OH})^+$  probably tends to hydrate due to the hydrogen bond interaction between  $\text{H}_2\text{O}$  and hydroxy. Accordingly, the difference in  $\text{NO}_x$  storage capacities of  $\text{Z}^- - \text{Pd}(\text{OH})^+$  and  $\text{Z}^- - \text{Pd}^{2+} - \text{Z}^-$  is probably caused by the different resistance to  $\text{H}_2\text{O}$  in this condition.

The atom utilization of Pd can be represented by mole ratios of  $\text{NO}_x$  adsorbed to total Pd loading. According to Figure 6, the Pd utilization of 0.2-Pd is as much as 100% whereas that of 2-Pd is only 25%. So, it is obvious that lower Pd loading benefits to the increase of Pd utilization. Besides, Khivantsev et al. [13] have reported that the Pd utilization of the 1 wt% Pd/SSZ-13 (Si/Al ratio = 6) sample is 100%, which is much higher than that of 1-Pd (Si/Al ratio = 16) using BEA as a support. Accordingly, zeolite structure and Si/Al ratio can also influence the Pd utilization. In this part, only the influence of Pd loading will be discussed.

As discussed above, lower Pd loading leads to lower content of isolated  $\text{Pd}^{2+}$ , whereas the proportion of isolated Pd ions in total Pd loading becomes larger. On the one hand, a larger proportion of isolated Pd ions in total Pd loading is beneficial for the improvement of Pd utilization, since isolated Pd ions are identified as the main active center for  $\text{NO}_x$  storage. On the other hand, less isolated  $\text{Pd}^{2+}$  results in a preference for the formation of  $\text{Z}^- - \text{Pd}^{2+} - \text{Z}^-$  which exhibits higher  $\text{NO}_x$  storage capacity. Thus, the atom utilization of Pd can be improved by decreasing Pd loading.

Nevertheless, lower Pd loading also leads to less  $\text{NO}_x$  storage capacities of unit mass of Pd/BEA. Note that the coating amount of catalysts is limited in order to obtain acceptable back pressure. Accordingly, to determine optimum Pd loading for low temperature  $\text{NO}_x$  adsorption, the  $\text{NO}_x$  storage capacity and the atom utilization of Pd should be both considered. As shown in Figure 6, 0.2-Pd and 0.5-Pd exhibits much higher Pd atom utilization than that of the other two samples. Meanwhile, Pd atom utilization of 0.5-Pd is 92%, which is only slightly lower than that of 0.2-Pd. However, the  $\text{NO}_x$

storage capacity of 0.5-Pd is larger than twice of that of 0.2-Pd. So, 0.5wt% should be determined as the optimum Pd loading for Pd/BEA (Si/Al ratio = 16) served as PNA material.

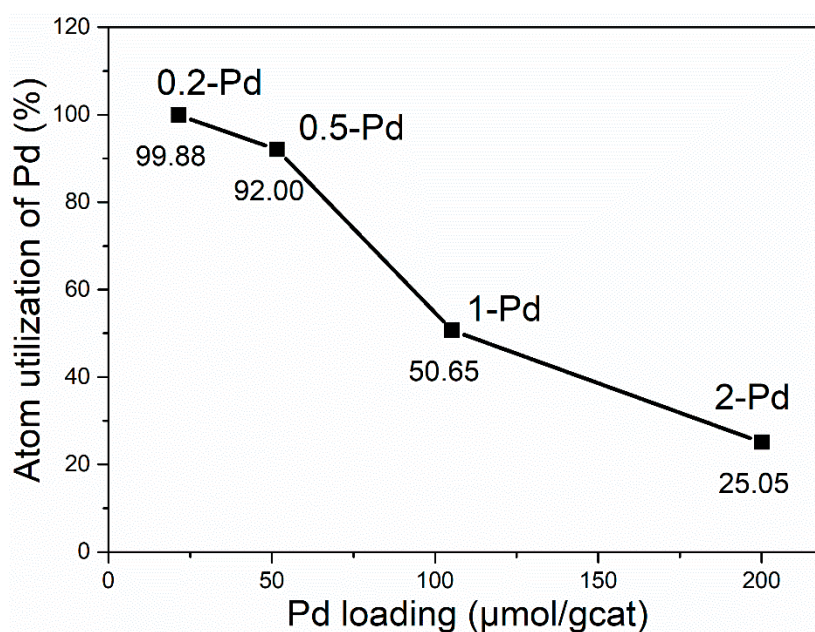


Figure 6. Tendency between Pd loading and the atom utilization of Pd.

### 3. Materials and Methods

#### 3.1. Catalyst Preparation

H-BEA zeolite (Si/Al = 16.2) was supplied by Novel Chemistry. Pd/BEA samples with various Pd loading were prepared by incipient wetness impregnation, and Pd(NO<sub>3</sub>)<sub>2</sub> solution (15.47wt% Pd, Heraeus Materials Technology Shanghai Ltd., Shanghai, China) was used. Then, the powders obtained were dried under ambient temperature followed by a 4-h calcination at 550 °C in air. Finally, samples were stabilized at 750 °C for 12 h in air with 10% H<sub>2</sub>O. Pd loading of each sample was detected by inductively coupled plasma (ICP) analysis (USA Agilent 5100 ICP-OES, Santa Clara, CA, USA). Si/Al ratios were measured by X-ray fluorescence (XRF, ThermoFisher PERFORM'X, Waltham, MA, USA) analysis. Detailed information is exhibited in Table 3. In the following text, samples are abbreviated as *x*-Pd, where “*x*” represents the Pd loading of corresponding samples. Besides, the sample treated by Na<sup>+</sup> titration was named as Na-1-Pd.

Table 3. Pd loading of samples.

Catalyst	0-Pd	0.2-Pd	0.5-Pd	1-Pd	2-Pd	Na-1-Pd
ICP Pd (wt %)	0	0.23	0.55	1.12	2.13	0.25

#### 3.2. Catalyst Characterization

Na<sup>+</sup> titration was used to quantify isolated Pd ions as reported by Ogura et al. [23]. Each sample was mixed with NaNO<sub>3</sub> (Purity above 99.0%, Tianjin Jiangtian Chemical Technology Co., Ltd., Tianjin, China) solution (0.1M) at 80 °C. The solution was stirred for 4 h followed by suction filtration. At last, the powders obtained were washed by deionized water and dried at 100 °C for 6 h. The whole process above was repeated three times. By analyzing the change of Pd loading in each sample after the titration process, the content of isolated Pd can be measured.

NO<sub>x</sub> storage capacities were measured by standard catalyst evaluation tests carried out in a plug flow reactor system. 0.25 g sample (60–80 mesh) mixed with 0.75 g quartz (60–80 mesh) was loaded in

a quartz reactor with a thermocouple. The sample was oxidized in the flow of 10% O<sub>2</sub>/N<sub>2</sub> for 30 min at 500 °C and was cooled to 80 °C in N<sub>2</sub>. Then the flow (200 ppm NO<sub>x</sub>, 200 ppm CO, 5% CO<sub>2</sub>, 5% H<sub>2</sub>O, 10% O<sub>2</sub>, balanced with N<sub>2</sub>) mixed in the bypass in advance was introduced into the reactor. The NO<sub>x</sub> adsorption stage continued for 3 min. After that, the sample was heated to 500 °C with a ramping rate of 10 °C/min in the flow of N<sub>2</sub>. Gas concentrations were measured by an online MKS MultiGas 2030 FTIR gas analyzer in the whole process. Besides, a space velocity of 28,800 h<sup>-1</sup> was adopted.

Ex-situ FTIR was carried out on a Nicolet iS10 FTIR spectrometer equipped with a liquid N<sub>2</sub> cooled mercury cadmium telluride (MCT) detector to identify the existence of Pd ions. The sample (20 mg) was pressed into a self-supporting wafer with a diameter of 13 mm and was inserted into a cell sealed with ZnSe windows connected with a gas manifold. KBr was used to obtain background spectra. All samples, as well as KBr, were oxidized in the flow of 10% O<sub>2</sub>/N<sub>2</sub> for 30 min at 500 °C in advance. Spectra were obtained at 200 °C in N<sub>2</sub>.

In situ FTIR was carried out on a Nicolet iS10 FTIR spectrometer, too. Test temperatures and feed compositions varied according to the needs of different experiments, and detailed information will be reported below.

#### 4. Conclusions

In this work, two isolated Pd<sup>2+</sup> ions, Z<sup>-</sup>-Pd<sup>2+</sup>-Z<sup>-</sup> and Z<sup>-</sup>-Pd(OH)<sup>+</sup>, on exchange sites of zeolites are confirmed as the main active sites for NO trapping in cold-start applications. Lower Pd loading leads to a lower content of isolated Pd<sup>2+</sup> whereas the proportion of isolated Pd ions in total Pd loading becomes larger. Lower content of isolated Pd<sup>2+</sup> further leads to a sharp decline of Z<sup>-</sup>-Pd(OH)<sup>+</sup>, which is attributed to the 'exchange preference' for Z<sup>-</sup>-Pd<sup>2+</sup>-Z<sup>-</sup> in BEA. Besides, the higher NO<sub>x</sub> storage capacity of Z<sup>-</sup>-Pd<sup>2+</sup>-Z<sup>-</sup> is demonstrated compared with that of Z<sup>-</sup>-Pd(OH)<sup>+</sup>, which is caused by the different resistance to H<sub>2</sub>O. In conclusion, the atom utilization of Pd can be improved by using lower Pd loading. 0.5wt% should be determined as the optimum Pd loading for Pd/BEA (Si/Al ratio = 16) serving as PNA material among all samples.

**Supplementary Materials:** The following are available online at <http://www.mdpi.com/2073-4344/9/3/247/s1>, Table S1: Detailed information of 1-Pd-80, Figure S1: CO in situ FTIR spectra of 1-Pd-80, Figure S2: NO<sub>x</sub> adsorption profiles of 1-Pd and 1-Pd-80, Figure S3: NH<sub>3</sub> in situ FTIR spectra of 1-Pd-80.

**Author Contributions:** Conceptualization, B.Z.; methodology, J.W. (Jun Wang), M.S., and J.W. (Jianqiang Wang); software, B.Z.; validation, J.W. (Jianqiang Wang); formal analysis, J.W. (Jianqiang Wang); investigation, B.Z. and J.W. (Jiaming Wang); writing—original draft preparation, B.Z.; writing—review and editing, B.Z.; visualization, B.Z.; supervision, J.W. (Jun Wang); resources, M.S.; project administration, M.S.; funding acquisition, M.S.

**Funding:** This research was funded by National Key Research and Development Program, grant number 2017YFC0211002; State Key Laboratory of Advanced Technologies for Comprehensive Utilization of Platinum Metals, grant number SKL-SPM-2018017.

**Conflicts of Interest:** The authors declare no conflict of interest.

#### References

1. Johnson, T.; Joshi, A. Review of vehicle engine efficiency and emissions. *SAE Int. J. Engines* **2018**, *11*, 1307–1330.
2. Gao, F.; Tang, X.; Yi, H.; Zhao, S.; Li, C.; Li, J.; Shi, Y.; Meng, X. A Review on Selective Catalytic Reduction of NO<sub>x</sub> by NH<sub>3</sub> over Mn-Based Catalysts at Low Temperatures: Catalysts, Mechanisms, Kinetics and DFT Calculations. *Catalysts* **2017**, *7*, 199. [[CrossRef](#)]
3. Kubiak, L.; Matarrese, R.; Castoldi, L.; Lietti, L.; Daturi, M.; Forzatti, P. Study of N<sub>2</sub>O Formation over Rh- and Pt-Based LNT Catalysts. *Catalysts* **2016**, *6*, 36. [[CrossRef](#)]
4. Chen, H.-Y.; Collier, J.E.; Liu, D.; Mantarosie, L.; Durán-Martín, D.; Novák, V.; Rajaram, R.R.; Thompson, D. Low temperature NO storage of zeolite supported Pd for low temperature diesel engine emission control. *Catal. Lett.* **2016**, *146*, 1706–1711. [[CrossRef](#)]
5. Chen, H.-Y.; Mulla, S.; Weigert, E.; Camm, K.; Ballinger, T.; Cox, J.; Blakeman, P. Cold Start Concept (CSC<sup>TM</sup>) A Novel Catalyst for Cold Start Emission Control. *SAE Int. J. Fuels Lubr.* **2013**, *6*, 372–381. [[CrossRef](#)]

6. Ryou, Y.; Lee, J.; Cho, S.J.; Lee, H.; Kim, C.H.; Kim, D.H. Activation of Pd/SSZ-13 catalyst by hydrothermal aging treatment in passive NO adsorption performance at low temperature for cold start application. *Appl. Catal. B* **2017**, *212*, 140–149. [[CrossRef](#)]
7. Lee, J.; Ryou, Y.; Hwang, S.; Kim, Y.; Cho, S.J.; Lee, H.; Kim, C.H.; Kim, D.H. Comparative study of the mobility of Pd species in SSZ-13 and ZSM-5, and its implication for their activity as passive NO<sub>x</sub> adsorbers (PNAs) after hydro-thermal aging. *Catal. Sci. Technol.* **2019**, *9*, 163–173. [[CrossRef](#)]
8. Ryou, Y.; Lee, J.; Lee, H.; Kim, C.H.; Kim, D.H. Effect of various activation conditions on the low temperature NO adsorption performance of Pd/SSZ-13 passive NO<sub>x</sub> adsorber. *Catal. Today* **2019**, *320*, 175–180. [[CrossRef](#)]
9. Vu, A.; Luo, J.; Li, J.; Epling, W.S. Effects of CO on Pd/BEA Passive NO<sub>x</sub> Adsorbers. *Catal. Lett.* **2017**, *147*, 745–750. [[CrossRef](#)]
10. Zheng, Y.; Kovarik, L.; Engelhard, M.H.; Wang, Y.; Wang, Y.; Gao, F.; Szanyi, J. Low-Temperature Pd/Zeolite Passive NO<sub>x</sub> Adsorbers: Structure, Performance, and Adsorption Chemistry. *J. Phys. Chem. C* **2017**, *121*, 15793–15803. [[CrossRef](#)]
11. Lee, J.; Ryou, Y.; Cho, S.J.; Lee, H.; Kim, C.H.; Kim, D.H. Investigation of the active sites and optimum Pd/Al of Pd/ZSM-5 passive NO adsorbers for the cold-start application: Evidence of isolated-Pd species obtained after a high-temperature thermal treatment. *Appl. Catal. B* **2018**, *226*, 71–82. [[CrossRef](#)]
12. Khivantsev, K.; Gao, F.; Kovarik, L.; Wang, Y.; Szanyi, J. Molecular Level Understanding of How Oxygen and Carbon Monoxide Improve NO<sub>x</sub> Storage in Palladium/SSZ-13 Passive NO<sub>x</sub> Adsorbers: The Role of NO+ and Pd (II)(CO)(NO) Species. *J. Phys. Chem. C* **2018**, *122*, 10820–10827. [[CrossRef](#)]
13. Khivantsev, K.; Jaegers, N.R.; Kovarik, L.; Hanson, J.C.; Tao, F.; Tang, Y.; Zhang, X.; Koleva, I.Z.; Aleksandrov, H.A.; Vayssilov, G.N.; et al. Achieving Atomic Dispersion of Highly Loaded Transition Metals in Small-Pore Zeolite SSZ-13: High-Capacity and High-Efficiency Low-Temperature CO and Passive NO<sub>x</sub> Adsorbers. *Angew. Chem.* **2018**, *130*, 16914–16919. [[CrossRef](#)]
14. Mei, D.; Gao, F.; Szanyi, J.; Wang, Y. Mechanistic insight into the passive NO<sub>x</sub> adsorption in the highly dispersed Pd/HBEA zeolite. *Appl. Catal. A* **2019**, *569*, 181–189. [[CrossRef](#)]
15. Khivantsev, K.; Jaegers, N.R.; Kovarik, L.; Proding, S.; Derewinski, M.A.; Wang, Y.; Gao, F.; Szanyi, J. Palladium/Beta zeolite passive NO<sub>x</sub> adsorbers (PNA): Clarification of PNA chemistry and the effects of CO and zeolite crystallite size on PNA performance. *Appl. Catal. A Gen.* **2019**, *569*, 141–148. [[CrossRef](#)]
16. Ryou, Y.; Lee, J.; Kim, Y.; Hwang, S.; Lee, H.; Kim, C.H.; Kim, D.H. Effect of reduction treatments (H<sub>2</sub> vs. CO) on the NO adsorption ability and the physicochemical properties of Pd/SSZ-13 passive NO<sub>x</sub> adsorber for cold start application. *Appl. Catal. A* **2019**, *569*, 28–34. [[CrossRef](#)]
17. Porta, A.; Pellegrinelli, T.; Castoldi, L.; Matarrese, R.; Morandi, S.; Dzwigaj, S.; Lietti, L. Low Temperature NO<sub>x</sub> Adsorption Study on Pd-Promoted Zeolites. *Top. Catal.* **2018**, *61*, 2021–2034. [[CrossRef](#)]
18. Theis, J.R.; Lambert, C.K. Mechanistic assessment of low temperature NO<sub>x</sub> adsorbers for cold start NO<sub>x</sub> control on diesel engines. *Catal. Today* **2019**, *320*, 181–195. [[CrossRef](#)]
19. Newsam, J.; Treacy, M.M.; Koetsier, W.; De Gruyter, C. Structural characterization of zeolite beta. *Proc. R. Soc. Lond. A* **1988**, *420*, 375–405. [[CrossRef](#)]
20. Gao, F.; Washton, N.M.; Wang, Y.; Kollár, M.; Szanyi, J.; Peden, C.H. Effects of Si/Al ratio on Cu/SSZ-13 NH<sub>3</sub>-SCR catalysts: Implications for the active Cu species and the roles of Brønsted acidity. *J. Catal.* **2015**, *331*, 25–38. [[CrossRef](#)]
21. Giordanino, F.; Vennestrøm, P.N.; Lundegaard, L.F.; Stappen, F.N.; Mossin, S.; Beato, P.; Bordiga, S.; Lamberti, C. Characterization of Cu-exchanged SSZ-13: A comparative FTIR, UV-Vis, and EPR study with Cu-ZSM-5 and Cu-β with similar Si/Al and Cu/Al ratios. *Dalton Trans.* **2013**, *42*, 12741–12761. [[CrossRef](#)] [[PubMed](#)]
22. Gao, F.; Peden, C.H.F. Recent Progress in Atomic-Level Understanding of Cu/SSZ-13 Selective Catalytic Reduction Catalysts. *Catalysts* **2018**, *8*, 140.
23. Ogura, M.; Hayashi, M.; Kage, S.; Matsukata, M.; Kikuchi, E. Determination of active palladium species in ZSM-5 zeolite for selective reduction of nitric oxide with methane. *Appl. Catal. B* **1999**, *23*, 247–257. [[CrossRef](#)]
24. Kumar, A.; Buttry, D.A. Influence of Halide Ions on Anodic Oxidation of Ethanol on Palladium. *Electrocatalysis* **2016**, *7*, 201–206. [[CrossRef](#)]

25. Yuan, N.; Pascanu, V.; Huang, Z.; Valiente, A.; Heidenreich, N.; Leubner, S.; Inge, A.K.; Gaar, J.; Stock, N.; Persson, I. Probing the evolution of palladium species in Pd@ MOF catalysts during the Heck coupling reaction: An operando X-ray absorption spectroscopy study. *J. Am. Chem. Soc.* **2018**. [[CrossRef](#)] [[PubMed](#)]
26. Palazov, A.; Chang, C.; Kokes, R. The infrared spectrum of carbon monoxide on reduced and oxidized palladium. *J. Catal.* **1975**, *36*, 338–350. [[CrossRef](#)]
27. Aylor, A.W.; Lobree, L.J.; Reimer, J.A.; Bell, A.T. Investigations of the Dispersion of Pd in H-ZSM-5. *J. Catal.* **1997**, *172*, 453–462. [[CrossRef](#)]
28. Okumura, K.; Amano, J.; Yasunobu, N.; Niwa, M. X-ray absorption fine structure study of the formation of the highly dispersed PdO over ZSM-5 and the structural change of Pd induced by adsorption of NO. *J. Phys. Chem. B* **2000**, *104*, 1050–1057. [[CrossRef](#)]
29. Barzetti, T.; Selli, E.; Moscotti, D.; Forni, L. Pyridine and ammonia as probes for FTIR analysis of solid acid catalysts. *J. Chem. Soc. Faraday Trans.* **1996**, *92*, 1401–1407. [[CrossRef](#)]
30. Pawelec, B.; Campos-Martin, J.; Cano-Serrano, E.; Navarro, R.; Thomas, S.; Fierro, J. Removal of PAH compounds from liquid fuels by Pd catalysts. *Environ. Sci. Technol.* **2005**, *39*, 3374–3381. [[CrossRef](#)] [[PubMed](#)]
31. Centeno, M.; Carrizosa, I.; Odriozola, J. NO–NH<sub>3</sub> coadsorption on vanadia/titania catalysts: Determination of the reduction degree of vanadium. *Appl. Catal. B* **2001**, *29*, 307–314. [[CrossRef](#)]
32. Niwa, M.; Nishikawa, S.; Katada, N. IRMS–TPD of ammonia for characterization of acid site in  $\beta$ -zeolite. *Microporous Mesoporous Mater.* **2005**, *82*, 105–112. [[CrossRef](#)]
33. Datka, J.; Gil, B.; Kubacka, A. Acid properties of NaH-mordenites: Infrared spectroscopic studies of ammonia sorption. *Zeolites* **1995**, *15*, 501–506. [[CrossRef](#)]
34. Ding, K.; Gulec, A.; Johnson, A.M.; Schweitzer, N.M.; Stucky, G.D.; Marks, L.D.; Stair, P.C. Identification of active sites in CO oxidation and water-gas shift over supported Pt catalysts. *Science* **2015**, *350*, 189. [[CrossRef](#)] [[PubMed](#)]
35. Bare, S.R.; Kelly, S.D.; Sinkler, W.; Low, J.J.; Modica, F.S.; Valencia, S.; Corma, A.; Nemeth, L.T. Uniform catalytic site in Sn- $\beta$ -Zeolite determined using x-ray absorption fine structure. *J. Am. Chem. Soc.* **2005**, *127*, 12924–12932. [[CrossRef](#)] [[PubMed](#)]
36. Jones, A.J.; Iglesia, E. The strength of Brønsted acid sites in microporous aluminosilicates. *ACS Catal.* **2015**, *5*, 5741–5755. [[CrossRef](#)]
37. Higgins, J.; LaPierre, R.B.; Schlenker, J.; Rohrman, A.; Wood, J.; Kerr, G.; Rohrbaugh, W. The framework topology of zeolite beta. *Zeolites* **1988**, *8*, 446–452. [[CrossRef](#)]



© 2019 by the authors. Licensee MDPI, Basel, Switzerland. This article is an open access article distributed under the terms and conditions of the Creative Commons Attribution (CC BY) license (<http://creativecommons.org/licenses/by/4.0/>).